

Journal of Materials Chemistry A

Accepted Manuscript



This is an *Accepted Manuscript*, which has been through the Royal Society of Chemistry peer review process and has been accepted for publication.

Accepted Manuscripts are published online shortly after acceptance, before technical editing, formatting and proof reading. Using this free service, authors can make their results available to the community, in citable form, before we publish the edited article. We will replace this *Accepted Manuscript* with the edited and formatted *Advance Article* as soon as it is available.

You can find more information about *Accepted Manuscripts* in the [Information for Authors](#).

Please note that technical editing may introduce minor changes to the text and/or graphics, which may alter content. The journal's standard [Terms & Conditions](#) and the [Ethical guidelines](#) still apply. In no event shall the Royal Society of Chemistry be held responsible for any errors or omissions in this *Accepted Manuscript* or any consequences arising from the use of any information it contains.

Cite this: DOI: 10.1039/c0xx00000x

www.rsc.org/xxxxxx

ARTICLE TYPE

LaFeO₃-based nanopowders prepared by a soft-hard templating approach: the effect of silica texture

Francesca Deganello,*^a Maria Luisa Testa,^a Valeria La Parola,^a Alessandro Longo,^{a,b} and Ana C. Tavares^c

Received (in XXX, XXX) Xth XXXXXXXXX 20XX, Accepted Xth XXXXXXXXX 20XX
DOI: 10.1039/b000000x

A combined soft-hard templating (SHT) approach was used to prepare LaFeO₃-based perovskite nanopowders with high surface area and porosity. In the SHT approach, a self-sustained combustion process between a soft fuel (citric acid) and an oxidant (metal nitrates) occurs in the presence of a silica hard template (amorphous, HMS or SBA-15 silica). The as-burned powders were then calcined, processed by basic etching and carefully characterized by X-ray diffraction combined with Rietveld refinement, small angle X-ray scattering, neutron activation analysis, N₂-adsorption, X-ray photoelectron spectroscopy and transmission electron microscopy. It was observed that structural, microstructural and textural properties of the obtained nanopowders strongly depend on the hard template used and an excellent correlation was found between the samples' specific surface area and cumulative pore volume of the original hard template. The use of several complementary characterization techniques revealed the composite nature of the prepared materials, evidencing the presence of amorphous La and Fe silicates in all the LaFeO₃ nanopowders. Furthermore, it was demonstrated that these silicates have an important function in the transmission of the microstructural-morphological-textural features from the template to the final powder.

Introduction

In recent years there has been growing interest in the synthesis of inorganic oxides by using soft or hard templating strategies.^{1,2} The template synthesis has the main advantage of producing materials with specific textural and microstructural properties, according to the desired application of the materials.^{1,2} Soft templates may be organic compounds, like carboxylates,⁹ aminoacids,³ surfactants,⁴ polymers,⁵ ionic liquids,⁶ cotton fibers^{7,8} or polystyrene spheres,⁹ which are decomposed by subsequent thermal treatment.

An example of synthesis of inorganic oxide powders which makes use of a soft template, is the solution combustion synthesis, which usually produces powders with higher surface area and smaller size with respect to solid state synthesis methods.^{10,11} Solution combustion synthesis is a well-known preparation method based on the concepts of both propellant chemistry and sol-gel chemistry, where a self-sustained reaction between a combustion fuel and an oxidant occurs in the presence of metal precursors.^{10,11} The soft template has multiple roles in the process, because it acts as fuel, chelating and gelling agent as well as microstructural template. The homogeneous chemical interaction between soft template and metal precursors before the combustion reaction is granted by the gel network formed in the presence of the gelling agent.

In the "nanocasting route", silica or carbon are commonly used

as hard templates to form silica (carbon)-inorganic oxide composites and, eventually, the final inorganic oxide material.^{2,12-18}

Among the inorganic oxides, perovskite compounds have attracted attention for their interesting functional properties, which are mainly due to their flexible crystallographic structure.^{19,20} The perovskite structure is able to accommodate a large variety of dopant ions and the properties of the final compound can be finely tuned through the careful choice of the dopant's type and amount.²⁰ Several structure classes exist with perovskite-structure, being the ABO₃-type the most studied one. Perovskite compounds with ABO₃-type structure have been intensively studied for their catalytic/electrocatalytic,^{14,17,21-24} magnetic²⁵ and gas-sensing properties.²⁶ Su *et al*¹⁴ synthesized a highly active LaFeO₃ photocatalysts with a specific surface area of 110 m²/g after calcination at 700°C using SBA-16 as template. Nair *et al*¹³ prepared ordered mesoporous LaFeO₃ and LaMnO₃ catalysts for methanol oxidation with a specific surface area of 101 m²/g and 155 m²/g, respectively, after calcination at 700°C using KIT-6 silica.

Here we present a facile solution combustion-based process combining a soft template like citric acid with a hard template like silica in a Soft-Hard Templating (SHT) approach for the preparation of LaFeO₃ nanopowders, to evaluate the influence of the templates on the properties of the final perovskite material. The substantial reduction of time/energy consuming step makes the combination of the two templating strategies a convenient

way to increase the efficiency of the classical hard templating methods, taking advantage of the simplicity and versatility of the solution combustion synthesis.

It is worth noticing that the SHT approach has not been employed before for the synthesis of perovskite powders. To the best of our knowledge, the use of auto-combustion in the presence of silica was reported only for the preparation of mixed oxides-silica composites such as perovskite-silica^{27,28} or spinel-silica.²⁹ Moreover, the experimental conditions, in terms of pH, combustion fuel, mixed oxide loading on silica, silica precursor and calcination temperature, were different by those used in this work.

In this work three types of silica with increasing surface area, cumulative pore volume and textural order were considered as hard templates in the SHT approach, in order to understand how the template's properties influence the phase composition, textural and microstructural properties of the perovskite material. For this purpose an amorphous silica (AS), a HMS silica (HMS) and a SBA-15 (SBA) silica were selected. AS and SBA have similar surface area, but different textural porosity and microstructural order; HMS and SBA are both high surface area and mesoporous, but only SBA shows an evidence of mesostructural order.

Materials and methods

Chemicals

All chemicals were purchased from Sigma-Aldrich and used without further purification: tetraethyl orthosilicate (TEOS, 99%), 1-dodecylamine, Pluronic P123 (MW=5800, EO₂₀PO₇₀EO₂₀), ethanol (99.8%), acetic acid (99.7%), La(NO₃)₃·6H₂O (99.999%), Fe(NO₃)₃·9H₂O (98%), citric acid (anhydrous), NH₄NO₃ (anhydrous), NH₄OH (solution, 30%vol.), NaOH (pellets).

Synthesis of the silica templates

The amorphous silica template (AS) was synthesized by sol-gel technique according to a published procedure.³⁰ TEOS (30 ml, 0.135 mol) was dissolved in ethanol (20 ml) and stirred at 45°C for 15 minutes. Then, 19 ml of aqueous solution of acetic acid at pH 5 was added to the mixture. The temperature was increased to 80°C until the formation of the gel. The obtained wet gel was dried at 110°C overnight and then calcined in air at 450°C/ 4 h. A surface area of 607 m²/g, a total pore volume of 0.384 cm³/g and a maximum pore diameter of 3.3 nm have been measured for the AS hard template.

The HMS silica template (HMS) was synthesized according to a previous published procedure.³¹ Typically, TEOS (12 ml, 0.054 mol) was added to a stirred solution of ethanol (31 ml), water (31 ml), and 1-dodecylamine (3.68 ml, 0.016 mol). The mixture was stirred at room temperature for 24 h. The white precipitate obtained was filtered under vacuum and washed with deionized water (36 ml) and ethanol (36 ml). The solid was dried at room temperature overnight, and then calcined in air at 600°C/4h. A surface area of 997 m²/g, a total pore volume of

0.447 cm³/g and a maximum pore diameter of 2.6 nm have been measured for the HMS hard template.

The SBA-15 silica template (SBA) was prepared by using as surfactant a non-ionic amphiphilic triblock polymer according to the procedures already described in the literature.^{32,33} Pluronic P123 (8.1 g) was dissolved in deionized water (146.8 ml) and HCl conc (37%, 4.4 g) and stirred overnight at 35°C in a 250 ml one neck flask. To this solution TEOS (17.1 ml, 0.077 mol) was quickly added and stirred for 24 h at 35°C. The milky suspension was aged at 100°C for 24 h in a closed PP bottle. The solid product was filtered, washed with an HCl/water mixture and calcined in air at 500°C/5h (heating ramp of 1°C/min). A surface area of 748 m²/g, a total pore volume of 1.009 cm³/g and a maximum pore diameter of 6.0 nm have been measured for the SBA hard template.

Synthesis of the LaFeO₃-based nanopowders

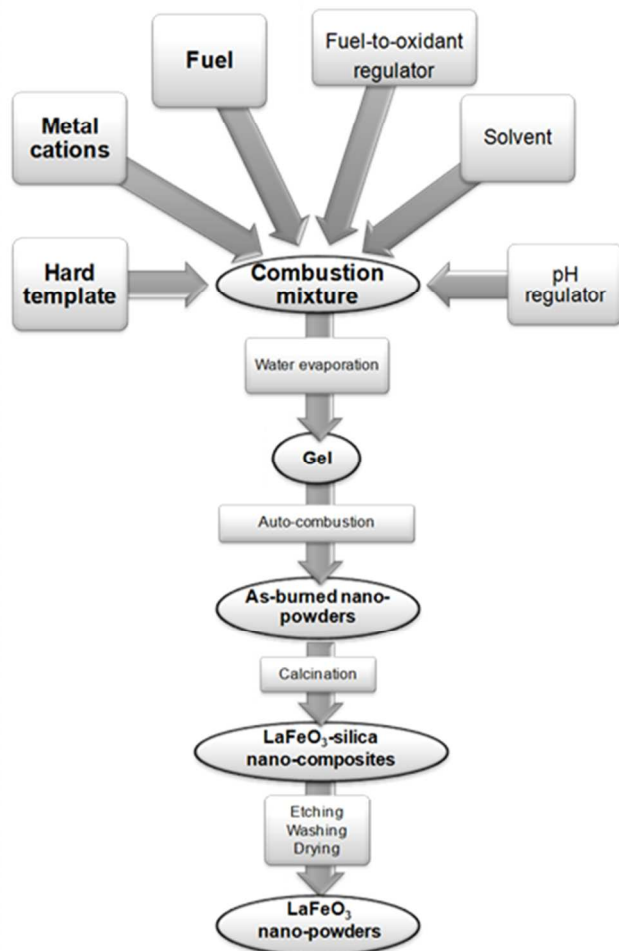
The steps required to synthesize the LaFeO₃ nanopowders by the SHT approach are schematically illustrated in Scheme 1. 1g of LaFeO₃ nano-powder was prepared as follows: La(NO₃)₃·6H₂O (1.783 g) and Fe(NO₃)₃·9H₂O (1.698 g) were dissolved in 150 ml of water in a 1 L stainless steel beaker. Citric acid (3.166 g), with citric acid/metal cations molar ratio=2, and NH₄NO₃ (2.770 g) were added as fuel-complexant and oxidant aid (fuel-to-oxidant molar ratio=0.28), respectively. The pH was adjusted to 5 with the aid of ammonia solution. Then, 1 g of silica template (silica/perovskite weight ratio = 1) was carefully poured in the beaker and the suspension was left stirring at 50°C to evaporate the water and to form the gel. After two hours, the temperature was raised to 80°C. The auto-combustion was initiated by increasing the hot-plate temperature to 250°C. The temperature profile of the reaction medium was recorded during the entire synthesis by means of a K-type thermocouple (1.5 mm in diameter) coupled with a data logger (PICO technology) with a sampling velocity of 20 bit/sec and a computer with Picolog software.

The obtained perovskite/silica composite powders were finally calcined at 700°C/5h with a heating ramp of 10°C/min. To etch the silica template, the composite was dispersed in NaOH solution (2M) and stirred for 3 hour at room temperature. The basic slurry (pH=12) was then filtered under vacuum, rinsed with NaOH solution, washed with distilled water until neutral pH and dried in the oven at 85°C/8h.

The powders are identified as LF-AS, LF-HMS and LF-SBA according to the template used in the SHT synthesis. A reference LaFeO₃ powder (LF) was also prepared by using the same synthetic procedure, but without adding any silica template.

Physicochemical characterization

X-ray diffraction (XRD) measurements were carried out on a Bruker-Siemens D5000 X-ray powder diffractometer equipped with a Kristalloflex 760 X-ray generator and with a curved graphite monochromator using the Cu K α radiation (40 kV/30 mA). A 2 θ scan range from 18° to 90° was considered, with a 2 θ step size of 0.03° and an integration time of 3 s per step. The



Scheme 1 Step-by-step description of the experimental procedure used in the SHT approach.

diffraction patterns were analyzed by Rietveld refinement using the GSAS package³⁴ and the agreement factors (“R values”)³⁵ were generally acceptable. Chebyshev polynomials and Pearson VII functions were chosen for the background and for the peak profile fitting, respectively. In the structure refinement lattice constants, zero offset, scale factors, full width half maximum (FWHM), Debye Waller factors and microstrain were considered as variable parameters. From fitting results, the structural parameters of the investigated compounds and, in particular, the cell edge lengths and the relative phase composition were obtained. The estimation of the crystal size values was done by using the Scherrer equation, in agreement with the GSAS package procedure³⁴. A standard deviation of $\pm 0.003 \text{ \AA}$ for the refined cell parameters was estimated in the experimental conditions used in this work.

The nitrogen adsorption/desorption technique was used to measure specific surface area (BET method) and mesopore size distributions (BJH method) at $-196 \text{ }^\circ\text{C}$, using a Sorptomatic 1900 Carlo Erba Instrument. All samples (ca. 0.110 g) were pre-treated under vacuum at $250 \text{ }^\circ\text{C}$ for 4 h prior to the measurements.

Neutron Activation Analysis (NAA) was applied for the evaluation of the bulk Si composition of the samples. The error in the chemical analysis is $\pm 5 \%$.

X-ray photoelectron spectroscopy (XPS) analyses were performed with a VGMicrotech ESCA 3000Multilab, equipped with a dual Mg/Al anode. The spectra were excited by the unmonochromatized Al $K\alpha$ source (1486.6 eV) run at 14 kV and 15 mA. The analyser was operated in the constant analyser energy (CAE) mode. For the individual peak energy regions, a pass energy of 20 eV set across the hemispheres was used. Survey spectra were measured at 50 eV pass energy. The sample powders were analyzed as pellets, mounted on a double-sided adhesive tape. The pressure in the analysis chamber was in the range of 10^{-8} Torr during data collection. The constant charging of the samples was removed by referencing all the energies to the C 1s set at 285.1 eV, arising from the adventitious carbon. The invariance of the peak shapes and widths at the beginning and at the end of the analyses ensured absence of differential charging. Analyses of the peaks were performed with the software provided by VG, based on non-linear least squares fitting program using a weighted sum of Lorentzian and Gaussian component curves after background subtraction according to Shirley³⁶ and Sherwood.³⁷ Atomic concentrations were calculated from peak intensity using the sensitivity factors provided with the software. The binding energy values are quoted with a precision of ± 0.15 eV and the atomic percentage with a precision of $\pm 10\%$.

Transmission electron microscopy (TEM) was employed to investigate the particles morphology. The TEM samples were prepared by dipping copper grids into dispersions of the powders in methanol and observed with a Transmission Electron Microscope JEOS-2100F operated at 200kV.

Small Angle X-ray Scattering (SAXS) measurements were carried out on a Bruker-Nanostar that is designed to have a very small footprint of only 950 mm x 2270 mm. Its compact 2-pinhole collimation system provides an intense beam of only 300 μm at the sample position, which is perfectly suited for analysing solid samples. The integration time to collect the 2D images was of about 300 s each. In order to analyze the data, the azimuthal average was performed with the BRUKER software, and the correspondently SAXS pattern was analyzed with an homemade program including the MINUIT package libraries.³⁸

Results and discussion

The visual observation of the combustion process in combination with the in-situ monitoring of the temperature as a function of the time, gives important information on the on-going of the self-sustained process. The addition of a silica template in the combustion mixture has an evident influence on the combustion process itself. In the absence of silica, the combustion was intense and it involved the whole mass of the gel (one single step), whereas in the presence of the silica templates, the gel ignition started at different points until complete burning of the mass. The difference in the intensity of the combustion process was confirmed by the temperature/time profiles and showed in Fig.1.

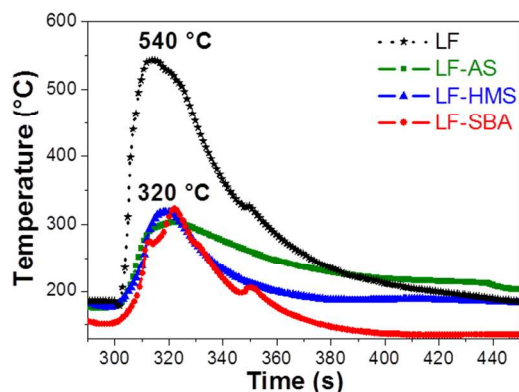


Fig. 1 Temperature/time profiles recorded during the combustion process of LaFeO_3 -based nanopowders prepared with (full lines with squares/AS, triangles/HMS or circles/SBA) and without (dotted line with stars) silica templates.

The maximum combustion temperature decreased from 540 °C in the absence of template to 320 °C for the SHT samples. This effect, probably due to the refractory properties of silica, was also noticed by Sellam *et al.*²⁷ for perovskite-silica composites prepared with smaller perovskite/silica weight ratio. On the other hand, no differences were evidenced among the temperature-time profiles registered for the SHT samples prepared from different silica templates.

15 Structural properties

In order to assess the influence of silica on the LaFeO_3 phase formation, XRDs were recorded just after the combustion step, after calcination at 700°C/ 5h, when a composite with silica was formed, and after the basic etching step (for SHT samples). Fig. 2 shows the diffractograms of the LF-SBA series as an example.

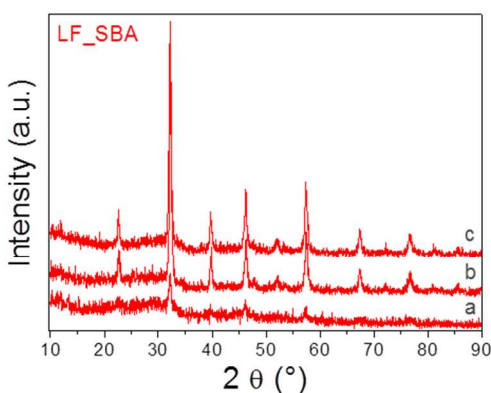


Fig. 2 XRD patterns of LF-SBA samples a) as-burned, (b) after calcinations at 700°C for 5h before etching and (c) after etching with NaOH.

All the examined XRD patterns can be assigned to the orthorhombic perovskite LaFeO_3 structure (ICSD #164083). However, the intensity of the diffraction peaks is very low in the case of the as-burned LF-SBA (pattern a), if compared with the

thermally treated LF-SBA powders (patterns b and c), indicating that the crystallization process of the perovskite is not yet completed after combustion. As it may be expected, the intensity of the perovskite's peaks increases after calcination at 700°C and it is not affected by the etching step. Similar trends were found for the diffractograms of the samples prepared using the other silica templates (Fig. S1), whereas the LF sample prepared without template was well crystallized already after combustion (Fig. S2a).

The X-ray diffractograms of the LF-AS, LF-HMS, LF-SBA samples after calcination and etching, and of the calcined reference LF are reported in Fig. 3a. Although the crystalline patterns fully correspond to those of the orthorhombic perovskite-type LaFeO_3 (ICSD #164083) with average values $a = 5.58 \text{ \AA}$, $b = 7.85 \text{ \AA}$, $c = 5.56 \text{ \AA}$ and cell volume of 243 \AA^3 , the type of template has a remarkable influence on the intensity of the peaks which decreases from $\text{LF} > \text{LF-AS} > \text{LF-HMS} > \text{LF-SBA}$. The mean crystal size, calculated by Rietveld refinement decreases in the same direction, from LF (41 nm) and LF-AS (45 nm) to LF-HMS (29 nm) and LF-SBA (22 nm). A careful inspection of the diffractograms puts in evidence a broad lump in the 26° to 31° 2θ interval (Fig. 3b).

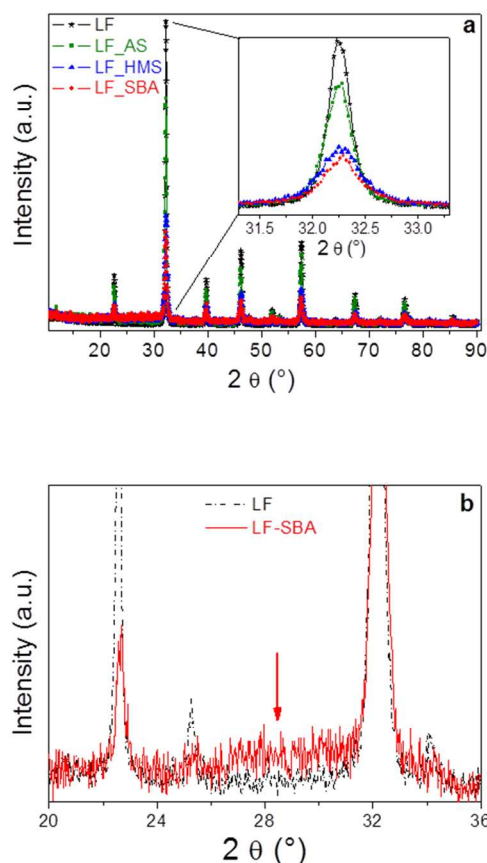


Fig. 3 (a) XRD patterns of LaFeO_3 -based nanopowders synthesized in the absence (LF) and in the presence of silica templates (LF-AS; LF-HMS; LF-SBA). Full lines with stars refer to the LF sample without template, squares to AS, triangles to HMS and circles to SBA. (b) Evidence of amorphous phases in the 26-31° 2θ range for the LF-SBA sample, as an example.

This lump is present in the diffractograms of the as-burned SHT samples and does not disappear after calcination at 700°C/5h, or after the basic etching. Moreover, this lump is not seen in the diffractograms of the as-burned and heat treated LF reference sample (Fig. S2).

Though it is clear that this amorphous contribution is formed during combustion step and only in the presence of silica, it cannot be ascribed to any of the silica templates as their diffraction features appear at another angular range (10-20° 2θ).

It is worth to notice that the amorphous content apparently increased in the following order: LF-AS < LF-HMS < LF-SBA.

With the aim at determining the nature and quantifying the amorphous contribution observed by XRD, the samples were further calcined at 800°C for 48h. After this thermal treatment the amorphous contribution became crystalline as shown in Fig. 4 for a representative SHT sample.

Rietveld analysis was used to fit the XRD patterns (details on the fitting results are summarized in Table S1), and, according to this analysis, the crystallized phases were identified as a mixture of iron and lanthanum silicates whose amount depends on the type of silica template originally used. The amount of mixed silicates increases in the order AS (12 wt%) < HMS (39 wt%) < SBA-15 (53 wt%) and for this later sample only 47 wt% is composed by pure LaFeO₃.

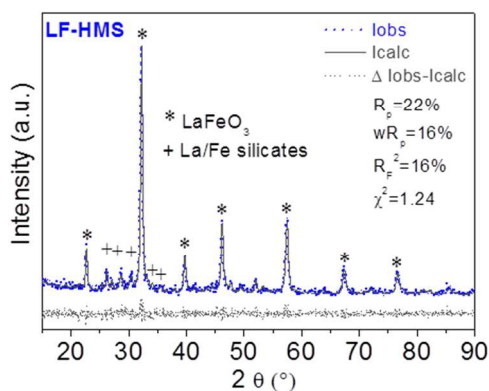


Fig. 4 Graphical Rietveld fit of LF-HMS after thermal treatment at 800°C/48h. Reliability factors are also reported in the figure.

Textural properties

The textural properties of all samples calcined at 700°C for 5h and then etched were analysed by recording nitrogen adsorption-desorption isotherms. The isotherms of LF, LF-AS and LF-HMS and LF-SBA are all of the type IV, as illustrated in Fig. 5 for LF-AS and LF-SBA, although they differ for the shape of the hysteresis loop.

LF-AS hysteresis, for example, is of the H1 type, indicative of an intra-particle porosity where the primary particles are essentially spherical (Fig. 5a). Differently, the LF-SBA hysteresis loop evidences the presence of both the typical mesoporous-like isotherm with a H3 type hysteresis, which is indicative of a sharp capillary condensation step inside slit pores at high relative pressures and the H1 type hysteresis, indicative of intra-particle porosity (Fig. 5b).

As expected, the SHT method led to nanopowders with surface

areas higher than the reference sample LF, as clearly indicated in Table 1. The highest specific surface area value, 168 m²/g, was obtained for LF-SBA and it was around 15 times higher than the one obtained in the absence of template (11 m²/g).

The small value of surface area measured for the LaFeO₃ prepared by solution combustion synthesis from citric acid and calcined at 700°C/5h is comparable with other values reported in the literature by using the classical citrate method¹⁴ or the glycine-nitrate auto-combustion.²⁷

Table 1 also reports the surface area (SA) calculated from the crystal size (CS) of the LaFeO₃ phase through the well known formula $SA=6/(CS \cdot \rho)$, where ρ is the theoretical density of the powder.³⁹

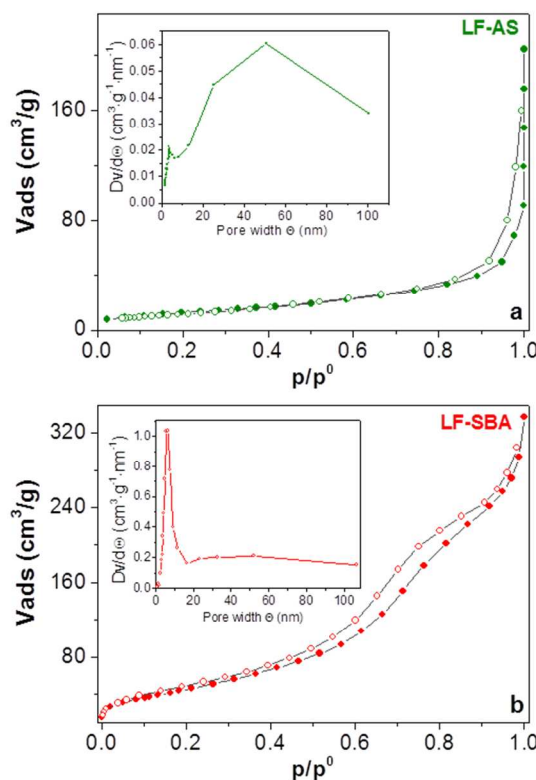


Fig. 5 Sorption isotherms and pore size distribution of LF-AS (a) and LF-SBA (b).

Table 1 Surface area (SA) (m²/g) from N₂ adsorption experiments in comparison with the surface area values calculated from the crystal size (CS) values extracted from the Rietveld refinement of the XRD patterns

Sample	SA (m ² /g)	SA (m ² /g)
name	from N ₂ adsorption	from XRD
LF	11	13
LF-AS	40	21
LF-HMS	78	35
LF-SBA	168	39

The comparison between SA values from N₂ adsorption and from XRD shows that the increase in SA of the nanopowders cannot be solely justified by a decrease of the crystal size of

LaFeO₃ phase.

The main contribution to the surface area is probably due to the amorphous silicate-phases cited in the previous paragraph. The pore volume of the four LaFeO₃-based nanopowders also increases in the order LF < LF-AS < LF-HMS < LF-SBA and the pore-size distribution is correspondently narrower (Fig. S3).

In addition, Fig. 6 also shows that the surface area and the cumulative pore volume of the SHT powders increase linearly with the cumulative pore volume of the original silica template. These trends clearly highlight the predominant effect of the silica template pore structure (pore volume and pore size) with respect to its specific surface area on the textural properties of the nanocasted materials.

The bulk Si content was quantified by neutral activation analysis (NAA), and it was found to be 1.72 wt% for LF-AS, 4.53 wt% for LF-HMS and 9.6 wt% for LF-SBA. NAA results suggest a correlation between the Si content with the type of silica template used in the SHT synthesis.

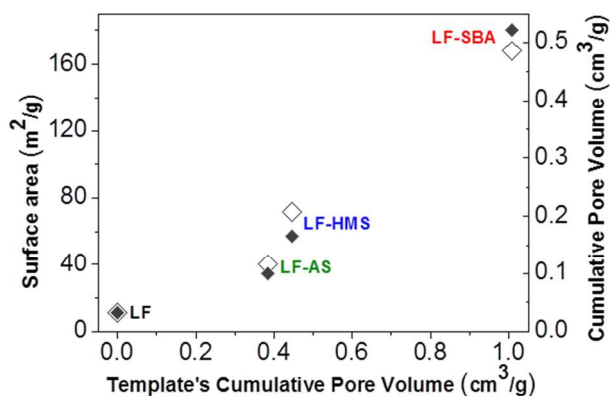


Fig. 6 Correlation between the specific surface area (large empty rhombs) and the cumulative pore volume (small full rhombs) of LaFeO₃-based nanopowders with the cumulative pore volume of the original silica template.

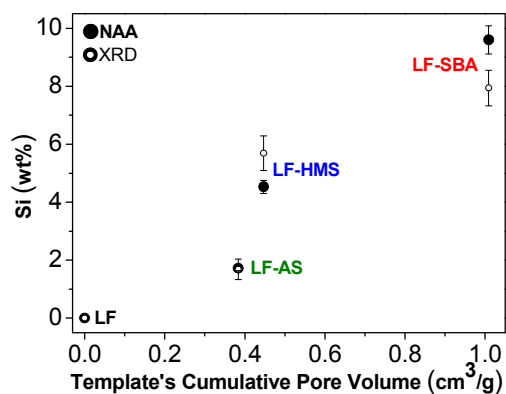


Fig. 7 Bulk Si wt% measured by neutron absorption analysis (large full circles) and determined from X-ray diffraction (small empty circles), as a function of the silica templates' cumulative pore volume. XRD data were obtained after Rietveld refinement of the XRD patterns of samples after thermal treatment at 800°C/48h. Error bars are also reported in the graphic.

The total Si wt% calculated by Rietveld refinement and by NAA was then correlated with the templates textural properties. As shown in Fig. 7 the Si wt% determined by the two methods agrees very well and it increases almost linearly with the cumulative pore volume of the original template. Therefore, it can be concluded that the silica template reacts with the metal precursors during the combustion process, and that the extent of reaction is proportional to the template's cumulative pore volume, or, in other words, to the extent of the interface formed between the template and the reactants.

Moreover, the mixed silicates probably contribute to the specific surface area and it cannot be ruled out that these secondary phases are responsible for the measured large values.

Therefore, it can be concluded that the silica template reacts with the metal precursors during the combustion process, and that the extent of reaction is proportional to the template's cumulative pore volume, or, in other words, to the extent of the interface formed between the template and the reactants. Moreover, the mixed silicates probably contribute to the specific surface area and it cannot be ruled out that these secondary phases are responsible for the measured large values.

Surface properties

The chemical state and surface composition of the LF samples calcined at 700°C for 5h and then etched were investigated by X-ray photoelectron spectroscopy. Details on the fitting results for Fe 2p_{3/2}, La 3d_{5/2}, O 1s are summarized in Table S2. The La 3d_{5/2} peaks centred at 834.5 eV show a satellite due to a transition from the anion valence band to a free lanthanum 4f state in the final state. The intensity ratio between satellite and main peak (α) is the same for all samples indicating that the different type of silica templates does not influence the chemical state of lanthanum. The binding energy of Fe 2p_{3/2} peak centred at 710.7 eV is typical of Fe(III) ions in oxidic form,²⁴ but all samples show a depletion of Fe in the surface. This behaviour has been observed already in similar system.⁴²

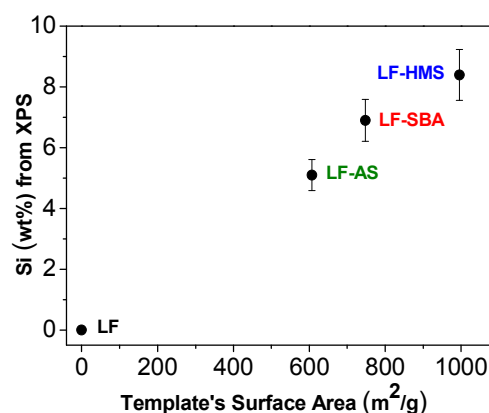


Fig. 8 Surface Si wt% calculated from XPS analysis as a function of the silica templates' specific surface area. Error bars are also reported in the graphic.

Si was found in the survey spectra of the nanopowders prepared by SHT method in addition to C, O, Fe and La. The more common peak for Si, the Si 2p, superimposes with the La

4d emission so, in this work, the Si 2s emission was chosen. The Si 2s peak (153.7 eV), which has the same value for all the investigated samples, is shifted of 1.4 eV from the SiO₂ template (155.3 eV) indicating that in the nanopowders Si is in a silicate environment. This result is in agreement with the trend discussed by Gaultois and Grosvenor for other transition metal amorphous silicates,⁴³ although in that case the chemical composition was different and the Si signal chosen was the more commonly used Si 2p. It is worth to note that the Si wt% calculated from XPS increases linearly with the specific surface area of the original template as illustrated in Fig. 8, indicating that the formation of superficial silicates depends on the hard template used and is favoured by templates with higher surface area. This result is not surprising since XPS is a surface technique and it is more influenced by the surface properties of the materials than by their bulk properties.

The O 1s peaks are wide and contain at least two kinds of O chemical states, Fig. 9.

The lower binding energy peak at around 529.5 eV can be ascribed to the lattice oxygen species.^{14,44} The higher binding energy peak at 531.5 eV is attributed to hydroxyl oxygen resulting mainly from the chemisorbed water.^{14,44} There are no evident changes in the relative percentage of the two forms of oxygen, although it is interesting to note the broadening of the oxygen peak in the SHT samples with respect to LF sample and according to the sequence LF < LF-AS < LF-HMS < LF-SBA (Table S2).

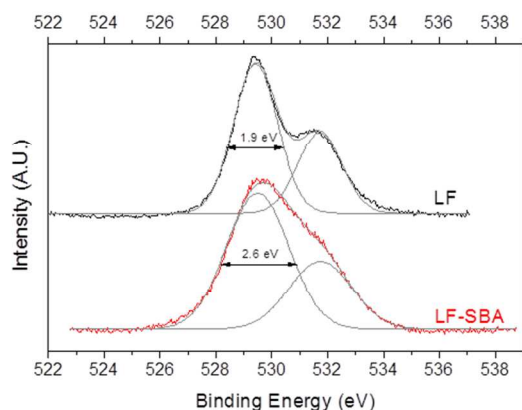


Fig. 9 Comparison between the O 1s XPS spectra of LF and LF-SBA nanopowders.

The broadening of the peaks results most probably from the additional contribution of oxygen from the silicates.

Microstructure and morphology

The first evidence from TEM results of the samples calcined at 700°C for 5h and then etched is that the particle size of the LF sample (Fig. S4a) is clearly larger than the particle size of the samples prepared by using a silica template (Fig. S4b,d and Fig. 10a). The inset of Fig.10a clearly shows that the LF-SBA nanoparticles are elongated, having a diameter which is much smaller than their length. The same elongation can be observed in Fig. S4d for LF-HMS, whereas this effect is much less evident in

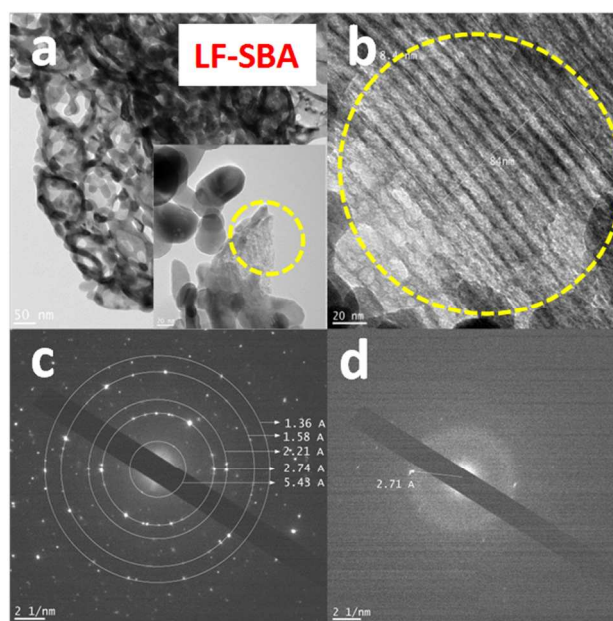


Fig. 10 (a) TEM images of LF-SBA powder, where the inset evidences the presence of a poorly crystalline region (yellow circle); (b) TEM image of the poorly crystalline region; (c) diffraction patterns of the crystalline region and (d) diffraction patterns of the poorly crystalline region.

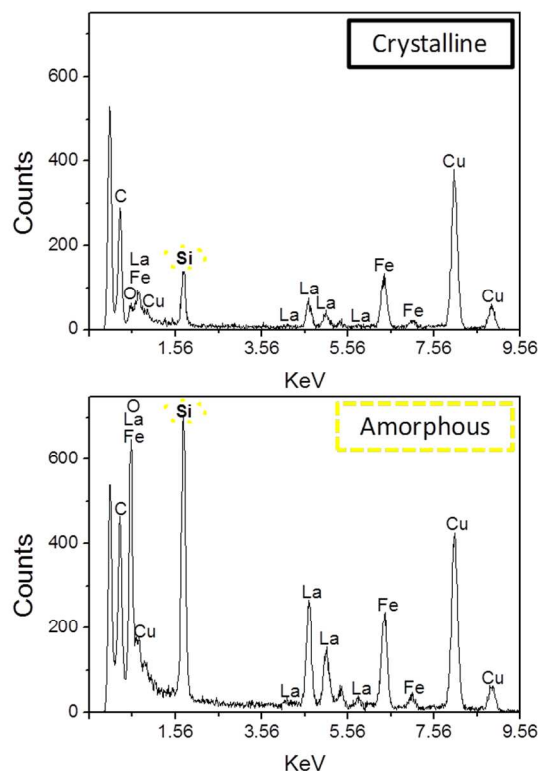


Fig. 11 Elemental analysis (EDX spectra) of crystalline and amorphous components of LaFeO₃-based nanopowders prepared using the SBA-15 silica template

LF-AS (Fig. S4b). This can be attributed to the formation of the perovskite particles inside the silica channels, although the

morphology of the particles depends very much on the type of silica used. Furthermore, amorphous regions near the crystalline domains could be spotted by TEM for LF-AS (Fig. S4c) and LF-HMS (Fig. S4e) samples, but not for the LF. It is interesting to note that in the case of the LF-SBA sample, which was prepared by using a SBA-15 template with microstructural order, only the amorphous component did replicate the template (Fig. 10a, b), for which a distance between the planes of 8.4 nm was measured (Fig. 10b).

The diffraction patterns shown in Fig. 10c, d confirmed the crystalline or amorphous structure by for the two TEM regions of LF-SBA. The diffraction pattern of Fig. 10c displays the typical diffraction features of a crystalline LaFeO_3 perovskite structure, whereas the diffraction pattern presented in Fig. 10d displays only one broad ring around 0.271 nm, indicating that this is an amorphous structure. Moreover, EDX analysis confirmed that the crystalline particles are essentially LaFeO_3 , whereas the amorphous domain is composed by La, Fe-silicates (Fig. 11).

All these findings are in excellent agreement with the XRD analysis presented above. In order to get information on the microstructural transition from the SBA-15 template to the final LF-SBA nano-powder, SAXS measurements and analysis were performed. The SAXS patterns of SBA-15 original template, LF-SBA_{BE} (before etching) and LF-SBA after etching are reported in Fig. 12.

The dashed line divides the patterns in two q ranges, denoting an amorphous zone in the q interval defined between 0.007 and 0.05 \AA^{-1} , and a crystalline-ordered zone between 0.05 and 0.3 \AA^{-1} .

The intensity and inclination of the diffraction signal in the first interval increases from the SBA-15 template, to the LF-SBA_{BE} and then to the etched LF-SBA nanopowder, confirming that the fraction of amorphous contribution is progressively increasing. On the other hand, the shape of this low q bump is quite similar for the three samples and, it can be attributed to particles whose inner porous structure has a 2D hexagonal packing, since the presence of pores larger than 80 nm was excluded by N_2 adsorption analysis.

Irrespective of the bump, the SAXS patterns of SBA-15 and LF-SBA_{BE} show the typical features of the 2D-hexagonal packing of parallel cylindrical pores (P6mmc crystallographic space group).⁴⁵ On the contrary, LF-SBA's pattern shows only a very broad peak pointing for a less well-ordered or even randomly distributed pore system. In addition, the two LF-SBA_{BE} and LF-SBA patterns have their main peak position shifted towards higher q values, with respect to the SBA-15 template. For what concerns LF-SBA_{BE}, this effect indicates a decreasing of the lattice parameter suggesting a decrease in size of the pores. In the case of the strongly disordered LF-SBA, the peak takes into account of the interference effect of the pores. So the shifting of the peak position is mainly due to the shrinking of the distance between the cylinders subunits.

In the 2D-hexagonal arrangement the lattice parameter a can be obtained from the q value of the most intense peak by using the relation $d_{10}=a(3)^{1/2}/2$ where d_{10} is the distance between the crystallographic planes (10). In addition, for this crystallographic system, assuming that pores are separated each other by the silica walls, it is possible to obtain the mean radius of the pore by using the relation $a \sim 2R+k$, where k is a parameter connected with the

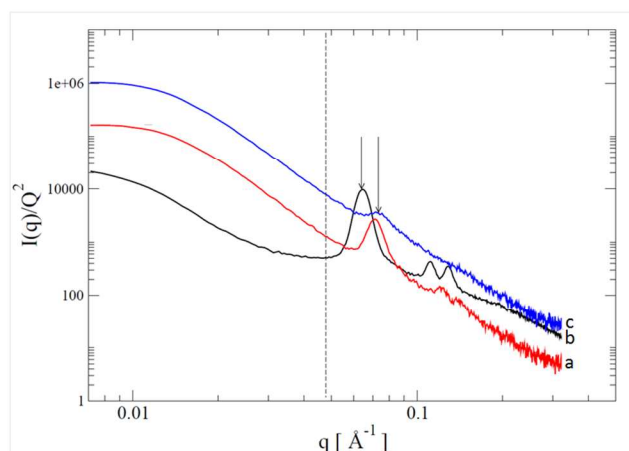


Fig. 12 The continuous black (a), red (b) and blue (c) lines are the SBA-15, the LF-SBA_{BE} (before etching) and the LF-SBA final powder, respectively. The arrows indicate the shift toward higher q values of the LF-SBA with respect to the original SBA-15 hard template.

silica wall thickness, which is $k/2$ (Table S3).

This procedure overestimates the pores dimensions, since the mean pore value calculated from N_2 -adsorption measurements is 6 nm for SBA-15 and it does not change very much for LF-SBA_{BE} and LF-SBA. Nevertheless, it still gives qualitative information on the system. However, this approach is not suitable for a disordered pore arrangement, so it cannot be used for LF-SBA.

For the less ordered or even randomly distributed pores, as in the case of the etched LF-SBA sample, a liquid-type structure factor was used to take into account the interference effects. To get quantitative information from this contribution, a Debye function typical of a bi-phase system was added to the main model (parallel cylindrical pores). The models, the main equations available in literature used for data analysis, the fitted spectra (Fig. S3) and the fitting parameters (Table S3) are reported in the Supporting Information. To the best of our knowledge, it is the first time that the liquid-type model is applied to solid systems. As evidenced in Table S3, the ordered domains of LF-SBA sample have a periodicity of 8.7 nm, in agreement with the distance between the planes of 8.4 nm observed by TEM (Fig. 10b). This means that the mesostructured domains evidenced by SAXS correspond to the silicate phase showed in the TEM figures. Moreover, as shown in Table S3 the pores radius decreases from the template (5 nm) to the etched sample (1.05 nm). This indicates that the pores of the mesostructured domains are contracted with respect to the original silica template. The roughness parameter σ_D increases in the different samples suggesting a coarsening of the cylindrical channels from the template to the etched sample, whereas a decrease of the dimensions of the ordered domains from 16.4 nm to 8.7 nm could suggest a partial filling of the channels. However, the presence of smaller pores after the etching treatment cannot be completely excluded.

The evidence of silicates in nanopowders prepared from silica hard template has been rarely reported and never clearly demonstrated in the literature. Nevertheless, according to the literature, it is well known that amorphous silicates can be easily formed due to the high chemical interaction of lanthanum or

cobalt with the silica template.^{13,46-49} Moreover, most of the recent literature papers about nanocasting of perovskite oxides from silica hard templates found an amorphous region in the TEM pictures and/or a 5 wt% residual Si% content after etching.^{50,13,15} It is thus reasonable to argue that a considerable amount of silicates is often present in the nanocasted oxide powders, although not always identified either because the amount of perovskite was too low with respect to the silica or because of a lack in the characterization of the powders concerning this particular aspect.

This work demonstrates, with complementary experimental evidences, that silicates form during the synthesis from silica templates and that they play a major role in the transmission of the microstructural, morphological and textural properties from the silica template to the final powder.

Conclusions

The soft-hard templating (SHT) route from silica templates is in principle a facile, simple and reproducible procedure for preparing LaFeO₃-based perovskite nanopowders with specific textural properties. It was clearly demonstrated that the presence of a silica hard-template in the combustion mixture has a marked influence both on the combustion process and on the structural, microstructural, textural and surface properties of the final nanopowders. It was found that amorphous La and Fe silicates are concomitantly formed with LaFeO₃ as a result of the strong interaction occurring between porous silica and metal cations during the combustion reaction. And even though after the etching procedure, the SiO₂ was completely removed, the La and Fe-silicates remained unaltered. For this reason, the original silica cannot be simply called “template”, if we consider a template as a molding material which is completely eliminated after its action. In this case, since silica acts both as a template and as a reagent, we address it as a *reactive template*.

High cumulative pore volumes of the silica *reactive template* favour the formation of silicates at the expenses of the perovskite phase, but produce LaFeO₃-based nanopowders with higher surface area. This makes the choice of the template essentially governed by the type of application of the final material.

The formed silicates are thought to play a major role in the transmission of the microstructural properties from the silica *reactive template* to the final powder, since they keep the microstructure of the original template favouring at the same time the dispersion of the perovskite onto the amorphous silicate porous framework.

By using the SHT approach, LaFeO₃-based perovskite materials with surface area up to 168 m²/g have been obtained. Furthermore, by using mesostructured *reactive templates* like SBA-15, LaFeO₃-based nanopowders with mesostructural order were formed, encouraging the use of the SHT method for all the cases where mesostructural order is relevant, for example, to heterogeneous catalysis applications. For the first time, a liquid-type model was successfully used for the analysis of the SAXS data of the mesostructurally ordered perovskite-based nanopowder. The results obtained in this work contribute substantially to elucidate the silica-perovskite interaction in nanocasted perovskite obtained using silica templates.

Acknowledgements

The authors are thankful to the STM Project 2010 (High surface area bifunctional catalysts for Zn-Air batteries) and NSERC (Canada) for funding. Dr. Francesco Giordano is also greatly acknowledged for the XRD and SAXS-measurements. Finally, the authors are grateful to Dr. Giuliana Magnacca for the fruitful discussion on the characterization of the textural properties.

Notes and references

- ⁶⁵ ^a *Istituto per lo Studio dei Materiali Nanostrutturati (ISMN) - Consiglio Nazionale delle Ricerche (CNR), UOS Palermo, Via Ugo La Malfa 153, 90146, Palermo, Italy. Fax: +39 091 6809399; Tel: +39 091 6809387; E-mails: francesca.deganello@cnr.it; valeria.laparola@cnr.it; marialuisa.testa@cnr.it; alessandro.longo@cnr.it.*
- ⁷⁰ ^b *Netherlands Organization for Scientific Research (NWO), DUBBLE@ESRF, 6 rue Jules Horowitz, BP220, 38043 Grenoble CEDEX, France. Fax: +33 4 7688 2412; Tel: +33 4 38881907; E-mail: alessandro.longo@esrf.fr.*
- ⁷⁵ ^c *Institute National de la Recherche Scientifique (INRS) – Energie, Matériaux et Télécommunications (EMT), 1650 Boulevard Lionel-Boulet, Varennes, Québec, Canada, J3X 1S2. Fax: +450 929 8102; Tel: +514 228 6947; E-mail: ana.tavares@emt.inrs.ca.*
- ⁸⁰ * *Corresponding author. email address.: francesca.deganello@cnr.it; telephone number.: +39-091-6809387; fax number.: +39-091-6809399.*
- ⁸⁵ † Electronic Supplementary Information (ESI) available: [Figures S1-S5; description of the SAXS model; references for the supplementary information; tables S1-S3]. See DOI: 10.1039/b000000x/
- 1 D. Gu, F. Schüth, *Chem. Soc. Rev.*, 2014, **43**, 313;
 - 2 M. Tiemann, *Chem. Mater.*, 2008, **20**, 961;
 - 3 R.R. Kondakindi, K. Karan, B.A. Peppley, *Ceram. Int.*, 2012, **38**, 449;
 - 4 N. Pal, A. Bhaumik, *Adv. Coll. Interface Sci.*, 2013, **189–190**, 21;
 - 5 N. Pal, M. Paul, A. Bhaumik, *Appl. Cat. A: Gen.*, 2011, **393**, 153;
 - 6 F.T. Li, Y. Liu, Z.M. Sun, R.H. Liu, C.G. Kou, Y. Zhao, D.S. Zhao, *Mater. Lett.*, 2011, **65**, 406;
 - 7 P. Li, X. Hu, L. Zhang, H. Dai, L. Zhang, *Nanoscale*, 2011, **3**, 974;
 - 8 P. Song, Q. Wang, Z. Zhang, Z. Yang, *Sens. Actuators B: Chem.*, 2010, **147**, 248;
 - 9 M. Sadakane, T. Horiuchi, N. Kato, K. Sasaki, W. Ueda, *J. Solid State Chem.*, 2010, **183**, 1365.
 - 10 F. Deganello, G. Marci, G. Deganello, *J. Eur. Ceram. Soc.*, 2009, **29**, 439;
 - 11 A.S. Mukasyan, P. Epstein, P. Dinka, *Proc. Comb. Inst.*, 2007, **31**, 1789;
 - 12 A.H. Lu, F. Schüth, *Adv. Mater.*, 2006, **18**, 1793;
 - 13 M.M. Nair, F. Kleitz, S. Kaliaguine, *Chem. Cat. Chem.*, 2012, **4**, 387;
 - 14 H. Su, L. Jing, K. Shi, C. Yao, H. Fu, *J. Nanopart. Res.*, 2010, **12**, 967;
 - 15 J. Zhao, Y. Liu, X. Li, G. Lu, L. You, X. Liang, F. Liu, T. Zhang, Y. Du, *Sensors and Actuators*, 2013, **8**, 802;
 - 16 N. Yi, Y. Cao, Y. Su, W.L. Dai, H.Y. He, K.N. Fan, *J. Catal.*, 2005, **230**, 249;
 - 17 J. Deng, L. Zhang, H. Dai, C.T. Au, *Appl. Cat. A: Gen.*, 2009, **352**, 43;
 - 18 O. Mihai, S. Raaen, D. Chen, A. Holmen, *J. Mater. Chem. A.*, 2013, **1**, 7006;
 - 19 A.S. Bhalla, R. Guo, R. Roy, *Mat. Res. Innovat.*, 2000, **4**, 3;
 - 20 A. Manthiram, J.H. Kim, Y.N. Kim, K.T. Lee, *J. Electroceram.*, 2011, **27**, 93;
 - 21 O. Mihai, D. Chen, A. Holmen, *Ind. Eng. Chem. Res.*, 2011, **50**, 2613;
 - 22 M.S. Hassan, K.B. Shim, O.B. Yang, *J. Nanosci. Nanotech.*, 2011, **11**, 1429;
 - 23 E. Campagnoli, A.C. Tavares, L. Fabbri, I. Rossetti, Y.A. Dubitsky, A. Zaopo, L. Forni, *J. Mater. Sci.*, 2006, **41**, 4713;

- 24 K.M. Parida, K.H. Reddy, D.P. Das, N. Biswal, *Int. J. Hydrogen Energy*, 2010, **35**, 12161;
- 25 M.B. Bellakki, V. Manivannan, *Bull. Mater. Sci.*, 2010, **33**, 611;
- 26 B.S. Li, S.B. Jie, M.L. Jing, Y.P. Cheng, L.Z. Yong, L.D. Qing, C.A. Fan, *Sci. China Ser. B: Chem.*, 2009, **52**, 2106;
- 27 D. Sellam, M. Bonne, S. Arrii-Clacens, G. Lafaye, N. Bion, S. Tezkraat, S. Royer, P. Marécot, D. Duprez, *Catal. Today*, 2010, **157**, 131;
- 28 M. Bonne, N. Bion, F. Pailloux, S. Valange, S. Royer, J.M. Tatibouët, D. Duprez, *Chem. Commun.*, 2008, **37**, 4504;
- 10 29 C. Cannas, A. Musinu, D. Peddis, G. Piccalunga, *J. Nanoparticle Res.*, 2004, **6**, 223;
- 30 G. Pecchi, P. Reyes, I. Concha, J.L.G. Fierro, *J. Catal.*, 1998, **179**, 309;
- 15 31 A.R. Silva, K. Wilson, J.H. Clark, C. Freire, *Micropor. Mesopor. Mater.*, 2006, **91**, 128;
- 32 M. Choi, W. Heo, F. Kleitz, R. Ryoo, *Chem. Commun.*, 2003, 1340;
- 33 D.Y. Zhao, Q.S. Huo, J.L. Feng, G.D. Chmelka, *J. Am. Chem. Soc.*, 1998, **120**, 6024;
- 20 34 A.C. Larson, R.B. Von Dreele, *GSAS, General Structure Analysis System*, LANSCE, MS-H805, Los Alamos National Laboratory: Los Alamos, NM 87545, USA, 1998;
- 35 L.B. McCusker, R.B. Von Dreele, D.E. Cox, D. Louer, P. Scardi, *J. Appl. Cryst.*, 1999, **32**, 36;
- 25 36 D.A. Shirley, *Phys. Rev. B Condens. Matter.*, 1972, **5**, 4709;
- 37 P.M.A. Sherwood, "Practical Surface Analysis" (D. Briggs and M. P. Seah, Eds.), 1990, 181. Wiley, New York.
- 38 F. James, *Fortran MINUIT Reference Manual*, Version 94.1, CERN Program Library Long Writeup D506;
- 30 39 P. Bowen, *J. Disper. Sci. Technol.*, 2002, **23**, 631;
- 40 W. Grunert, U. Sauerlandt, R. Schlögl, H.G. Karge, *J. Phys. Chem.*, 1993, **97**, 1413;
- 41 E.V. Makshina, S.V. Sirotnin, M.W.E. van den Berg, K.V. Klementiev, V.V. Yushchenko, G.N. Mazo, W. Grunert, B.V. Romanovsky, *Appl. Catal. A: Gen.*, 2006, **312**, 59;
- 35 42 J. Sfeir, S. Vaucher, P. Holtappels, U. Vogt, H.J. Schindler, J. Van Herle, E. Suvorova, P. Buffat, D. Perret, N. Xanthopoulos, O. Bucheli, *J. European Ceram. Soc.*, 2005, **25**, 1991;
- 43 M.G. Gaultois, A.P. Grosvenor, *Phys. Chem. Chem. Phys.*, 2012, **14**, 205;
- 40 44 A.C. Tavares, M.A.M. Cartaxo, M.I. da Silva Pereira, F.M. Costa, *J. Solid State Electrochem.*, 2001, **5**, 57;
- 45 W. Ruland, B. Smarsly, *Appl. Crystallogr.*, 2005, **38**, 78.
- 46 H. Vidal, S. Bernal, R.T. Baker, D. Finol, J.A. Perez Omil, J.M. Pintado, J.M. Rodríguez-Izquierdo, *J. Catal.*, 1999, **183**, 53;
- 45 47 Z. Sarshar, F. Kleitz, S. Kaliaguine, *Energy Environ. Sci.*, 2011, **4**, 4258;
- 48 F. Boubekr, A. Davidson, S. Casale, P. Massiani, *Micropor. Mesopor. Mater.*, 2011, **141**, 157;
- 50 49 M. Stoia, M. Stefanescu, T. Dippong, O. Stefanescu, P. Barvinschi, *J. Sol-Gel Sci. Technol.*, 2010, **54**, 49;
- 50 Y. Wang, X. Cui, Y. Li, L. Chen, Z. Shu, H. Chen, J. Shi, *Dalton Trans.*, 2013, **42**, 9448.